Journal of Materials Chemistry C

ROYAL SOCIETY OF CHEMISTRY

PAPER

View Article Online
View Journal | View Issue

Cite this: J. Mater. Chem. C, 2020, 8, 15183

Small-molecule electrolytes with different ionic functionalities as a cathode buffer layer for polymer solar cells†

Mijin Jeong,[a] Doo Kyung Moon,[b] Hyun Sung Kim*[c] and Joo Hyun Kim*[a]

Received 26th May 2020,
Accepted 8th July 2020

DOI: 10.1039/d0tc02513e

rsc.li/materials-c

In polymer solar cells (PSCs), electrolytes as the cathode interlayer are responsible for generating an interface dipole, which reduces the charge collection barrier at the cathode interface. In this study, small-molecule electrolytes were designed and synthesized as the cathode interlayer in inverted PSCs to overcome high processing costs caused by complicated synthesis procedures. Moreover, the proposed design strategy allows changing the ion size and number of ionic functionalities to tune the magnitude of the interface dipole. The structure of ((benzene-1,2,4,5-tetrayltetrakis(methylene))tetrakis(triphenylphosphonium) bromide) (**4PBr**) comprises a phenyl core with four benzyl triphenylphosphonium salts and (*N*,*N*′-(1,2-phenylenebis(methylene)) bis(*N*,*N*-diethylethanaminium) bromide) (**2EBr**) has two benzyl trialkyl ammonium salts. The device based on **4PBr** exhibited a power conversion efficiency of 10.63% (J_{sc} = 20.2 mA cm^{-2}, V_{oc} = 0.79 V, and FF = 66.6%), which is superior to that based on **2EBr** (PCE = 9.56%, J_{sc} = 19.7 mA cm^{-2}, V_{oc} = 0.80 V, and FF = 61.1%). Thus, we demonstrated the possibility of maximizing performances without complicated synthesis procedures.

Introduction

Over the last decade, there have been several approaches for developing highly efficient polymer solar cells (PSCs) due to their processability, flexibility, and low-cost fabrication for large-area applications.[1–4] Outstanding improvements with power conversion efficiencies (PCE) of up to 16%[5] have been achieved by developing efficient photoactive materials[6–16] and interface engineering the electrode.[17–37] Among the existing issues, tuning the energy offset at the cathode interface is an important issue that should be addressed to enhance the electron collection ability.

ZnO has been commonly used as the electron transport layer in inverted PSCs. To maximize its electron collection ability, there have been several approaches to change its layer properties, such as inserting conjugated/non-conjugated polymer electrolytes[17–30] as the interlayer and self-assembled monolayer[31–34] treatments. Thus, better PCEs were achieved by reducing the energy offset at the cathode interface and enhancing the charge collection capability.

Conjugated polymer electrolytes (CPEs) have been widely used as the cathode interlayer. However, CPEs have complicated synthetic procedures and extremely low product yield, thereby limiting their commercial large-area application. In terms of processing cost, the development of small-molecule organic electrolytes[38–45] with simple synthetic procedures can attract attention in large-area applications. Recently, we reported the effect of the size of the counter anion[36] and cation[46] of organic electrolytes on the photovoltaic properties. The results suggested that a larger counter ion leads to a larger interface dipole, indicating its influence on the energy offset at the cathode interface. Lee *et al.* and Jo *et al.* also reported that the number of ionic functionalities on electrolytes affect the performance of PSCs.[47–49] This suggests that the magnitude of the interface dipole depends on the number of ionic functionalities. Moreover, the increase in the size of ions and number of ionic functionalities has been observed to efficiently reduce the charge collection barrier at the interface, thereby improving device performances.

With these in mind, we have designed and synthesized (*N*,*N*′-(1,2-phenylenebis(methylene))bis(*N*,*N*-diethylethanaminium)-bromide) (**2EBr**) and ((benzene-1,2,4,5-tetrayltetrakis(methylene))-tetrakis(triphenylphosphonium)bromide) (**4PBr**) (shown in Fig. 1a). Both **2EBr** and **4PBr** have the advantage of allowing mass production without a complex synthetic procedure and low product yield. The dipole moment of the ionic compound is proportional to the distance between two charges. Therefore, the dipole moment of triphenyl phosphonium salt would be larger than that of triethyl ammonium salt. In addition to this, **4PBr** is expected to have a higher dipole moment than **2EBr** due to the number of ionic functionalities. The device based on a

[a] Department of Polymer Engineering, Pukyong National University, Busan 48513, Korea. E-mail: jkim@pknu.ac.kr
[b] Division of Chemical Engineering, Konkuk University, Seoul 05029, Korea
[c] Department of Chemistry, Pukyong National University, Busan 48513, Korea. E-mail: kimhs75@pknu.ac.kr

† Electronic supplementary information (ESI) available: Experimental details including materials, synthesis, measurements, and fabrication of devices. See DOI: 10.1039/d0tc02513e

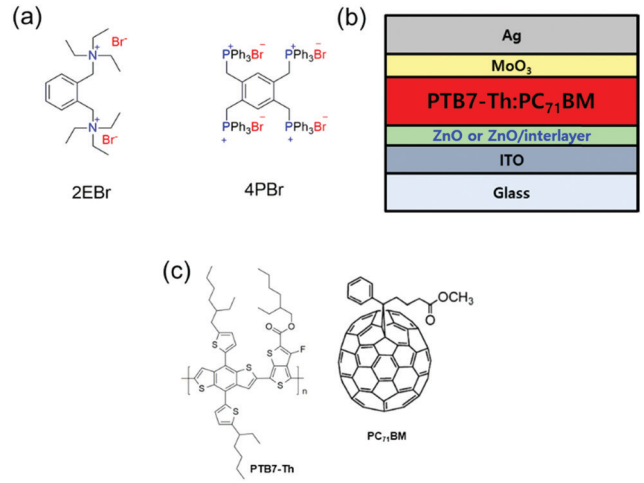

Fig. 1 Chemical structure of (a) small-molecule electrolytes and (b) PTB7-Th and $PC_{71}BM$. (c) Device structure of PSCs used in this study.

bulk-heterojunction structure (Fig. 1b) composed of poly([2,6′-4,8-di(5-ethylhexylthienyl)benzo[1,2-*b*;3,3-*b*]dithiophene]{3-fluoro-2[(2-ethylhexyl)carbonyl]thieno[3,4-*b*]thiophenediyl}) (PTB7-Th) and [6,6]-phenyl C71 butyric acid methyl ester ($PC_{71}BM$) (Fig. 1c) as the active layer enhances the PCE based on ZnO from 8.75% (short circuit current J_{sc} = 17.5 mA cm^{-2}, open circuit voltage V_{oc} = 0.80 V, and fill factor FF = 62.5%) to 10.63% (J_{sc} = 20.2 mA cm^{-2}, V_{oc} = 0.79 V, and FF = 66.6%), by introducing **4PBr** as the interlayer. Moreover, the device based on **4PBr** has a more superior PCE than that based on **2EBr** (PCE = 9.56%, J_{sc} = 19.7 mA cm^{-2}, V_{oc} = 0.80 V, and FF = 61.1%). This could be mainly attributed to the improved J_{sc} by the reduced Schottky barrier at the cathode interface.

Results and discussion

2EBr and **4PBr** were synthesized by a simple substitution reaction between 1,2-bis(bromomethyl)benzene and triethylamine in toluene and acetonitrile, respectively. All compounds were well characterized by the ^{1}H, ^{13}C NMR, and elemental analysis, which are provided in the ESI.†

We fabricated inverted type PSCs (illustrated in Fig. 1b) based on ZnO with and without small-molecule electrolytes as the electron transporting layer and investigated the effect of ionic functionalities on the photovoltaic properties. Detailed procedures of the fabrication of PSCs are described in the ESI† and the photovoltaic parameters with different thickness of the cathode interlayer are summarized in Table S1 (ESI†). The optimum thickness of the interlayer was determined to be 5–6 nm. As shown in Fig. S1 (ESI†), small-molecule electrolytes do not tend to aggregate on the surface of ZnO. The surface roughness of the ZnO surface with **2EBr** and **4PBr** was 0.58 and 0.60 nm, respectively, which are comparable to the surface roughness of the

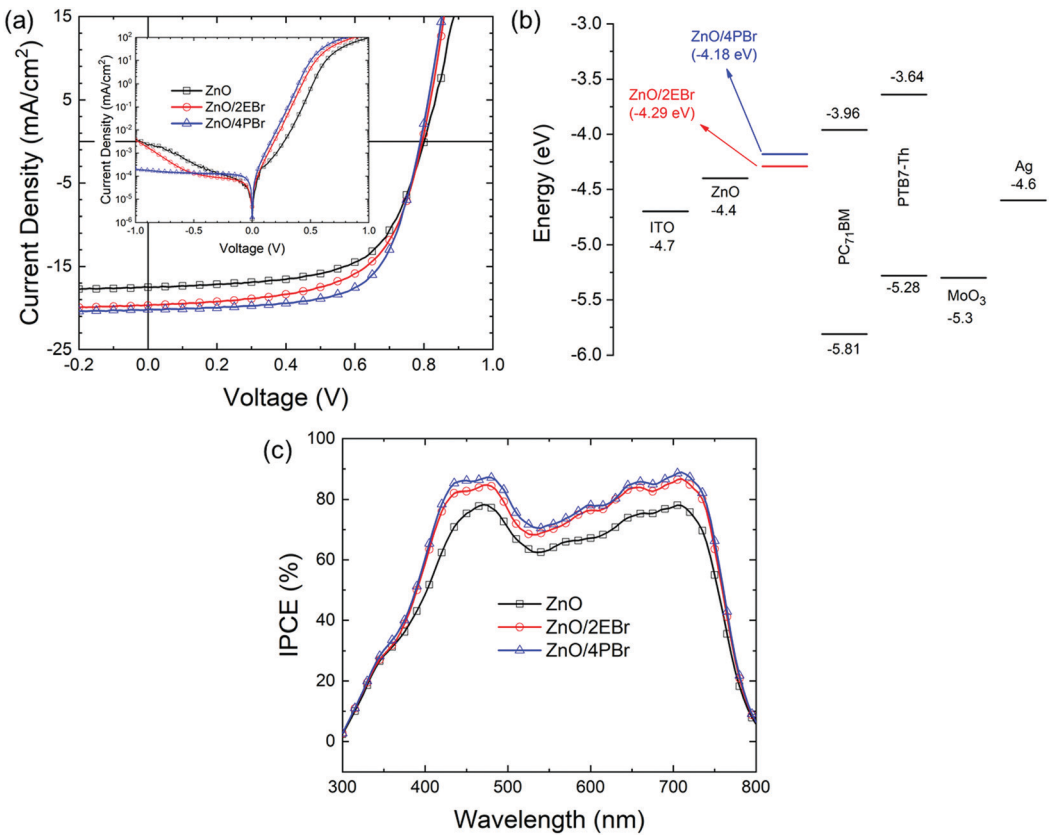

Fig. 2 (a) *J*–*V* curves and (b) energy level diagram of the materials and (c) incident photon to converted electron (IPCE) curves of the PSCs under the optimum processing conditions.

Table 1 Photovoltaic parameters of PSCs based on the ZnO/interlayer. The averages (10 devices) are shown in parentheses

Interlayer	J_{sc} (mA cm^{-2})	V_{oc} (V)	FF (%)	PCE (%)	$J_{sc,cal}$[a] (mA cm^{-2})	R_s[b] (Ω cm^2)	R_{sh}[b] (kΩ cm^2)
—	17.5 (17.3)	0.80 (0.80)	62.5 (62.7)	8.75 (8.69)	17.1	3.29	893
2EBr	19.7 (19.6)	0.80 (0.80)	61.1 (60.4)	9.56 (9.41)	19.1	2.60	645
4PBr	20.2 (20.1)	0.79 (0.79)	66.6 (65.2)	10.63 (10.29)	19.6	2.28	2533

[a] Calculated from IPCE curves. [b] Series and shunt resistance data are calculated from the device showing the best PCE.

ZnO surface (0.55 nm). Fig. 2a shows the current density–voltage (J–V) curves of PSCs with and without the interlayer under illumination while the photovoltaic performances are summarized in Table 1. Significant enhancements are observed in devices based on ZnO with an interlayer. The PCEs of devices with **2EBr** and **4PBr** are 9.56% (J_{sc} = 19.7 mA cm^{-2}, V_{oc} = 0.80 V, and FF = 61.1%) and 10.63% (J_{sc} = 20.2 mA cm^{-2}, V_{oc} = 0.79 V, and FF = 66.6%), while for that based on ZnO without the interlayer was limited to 8.75% (J_{sc} = 17.5 mA cm^{-2}, V_{oc} = 0.80 V, and FF = 62.5%). Notably, the enhanced J_{sc} was the main contributor to the improved PCE.

Kelvin probe microscopy (KPM) is a common powerful tool for determining the effective work function of a metal or metal oxide. Thus, KPM measurements were conducted to investigate how the interlayer affects the changes of J_{sc}.[21–23,26,27,36,37,42–46,48]

A larger Schottky barrier at the interface interrupts the charge collection capability.

Thus, the transition from a Schottky to ohmic contact at the interface is a crucial factor to achieve high J_{sc}. As shown in Fig. 2b, the work function of ZnO with **2EBr** and **4PBr** is −4.29 and −4.18 eV, respectively, while that of ZnO was −4.4 eV. The change in magnitude of the interface dipole depended on changing the size of the cation and number of ionic functionalities. Reducing the Schottky barrier height results in a high J_{sc}, which is strongly related to the change of work function. Herein, the improved J_{sc} indicates the formation of a favorable interface dipole with its magnitude depending on the ion size and number of ionic functionalities. The calculated J_{sc} data from IPCE curves (Fig. 2c) showed an extremely good correlation with the J_{sc} data of devices under a simulated illumination of 1.0 sun. The series resistance (R_s) and shunt resistance (R_{sh}) were calculated from the inverse slope near the high current regime and the slope near the lower current region in the dark J–V curves. The R_s data also showed its coherence with the J_{sc} of PSCs. The R_{sh} data of the device based on pure ZnO, and ZnO with **2EBr**, and **4PBr** were 893, 645, and 2553 kΩ cm^2, respectively, which are well correlated with their FF. Interestingly, the R_{sh} of the device based on **2EBr** was smaller than that without the interlayer.

To elucidate the effect of the interlayer on the electron transporting/collecting properties of ZnO, we fabricated and tested the electron devices with a structure of ITO/ZnO (25 nm)/ with or without the interlayer (60 nm)/$PC_{71}BM$/Al (100 nm) (Fig. 3). Fig. 3 shows the space-charge limited current (SCLC) characteristics of the current density and voltage. The electron mobilities of the devices were calculated by the SCLC method expressed by the Mott–Gurney law. The electron mobilities of the devices based on **2EBr** and **4PBr** were 9.2 × 10^{-4} and 1.2 × 10^{-3} cm^2 V^{-1} s^{-1}, respectively, which are comparable to the device

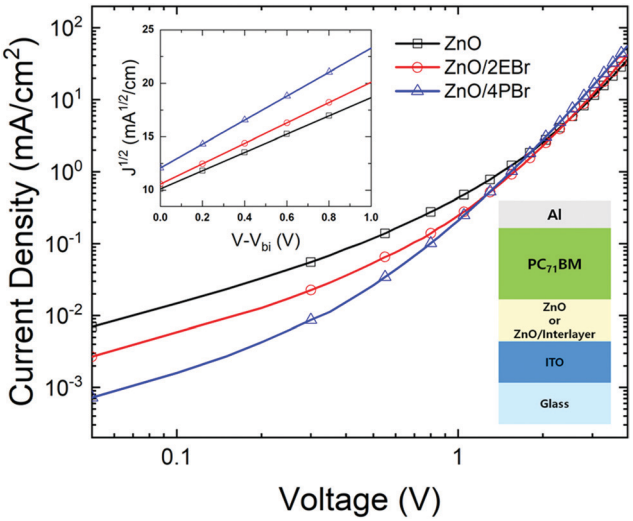

Fig. 3 Current density–voltage curves of electron-only devices with a configuration of ITO/ZnO (25 nm)/interlayer/$PC_{71}BM$ (60 nm)/Al (100 nm) (inset: with fitted line, V: applied voltage, and V_{bi}: built-in voltage).

based on ZnO without the interlayer (7.4 × 10^{-3} cm^2 V^{-1} s^{-1}). However, the turn-on voltages of the devices with **2EBr** and **4PBr**, which was estimated according to Parker,[49] were 1.26 and 0.94 V, respectively, while of that based on ZnO without the interlayer was limited to 1.65 V. Thus, the interlayer facilitates the electron collection capability from the $PC_{71}BM$ layer to the ZnO layer, owing to the introduced interlayer that reduced the Schottky barrier between them. Moreover, **4PBr** has easier electron collection ability than **2EBr**. These results are well coherent with the improvement of J_{sc}.

To understand the charge transport and collection properties of the devices, we analyzed the photocurrent density (J_{ph}) as a function of the effective voltage (V_{eff}) by:

$$J_{ph} = J_L - J_D$$

$$V_{eff} = V_0 - V_a$$

where J_L is the measured current density under illumination, J_D is the measured current density without illumination, V_0 is the voltage at J_{ph} = 0, and V_a is the applied voltage.

As shown in Fig. 4, the log(J_{ph}) as a function of log(V_{eff}) showed a linear relationship at low V_{eff} and saturated at the high V_{eff} regime. The V_{eff} value of the devices reaching the saturated photocurrent (V_{sat}) increased in the following order: **4PBr** (0.17 V) < **2EBr** (0.31 V) ≅ ZnO (0.34 V). Hence, a smaller V_{sat} denotes faster transition from the space-charge-limited to

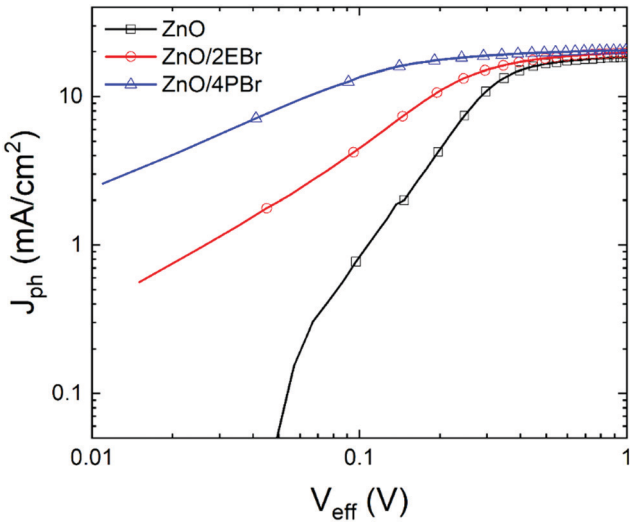

Fig. 4 J_{ph} as a function of V_{eff} curves in the PSCs.

the saturation regime. The results followed the trend of the J_{sc} and PCE of the devices.

We examined the J_{sc} and V_{oc} of the devices as a function of illumination intensity[50–52] to understand the charge recombination kinetics at the interfaces. The relationship between J_{sc} and illumination intensity I is generally defined by $J_{sc} \propto I^{\alpha}$. When the device exhibits a completely bimolecular recombination under short-circuit conditions, α is unity. As shown in Fig. 5a, the α of the devices based on ZnO with **2EBr** and **4PBr** is 0.97 for both, which is comparable to that based on ZnO (0.93). This indicates that the devices exhibited the suppression of undesirable bimolecular recombination. V_{oc} is defined by

$$V_{oc} \propto skT/q \cdot \ln(I)$$

where k, T, q, and I are the Boltzmann constant, temperature in Kelvin, electron charge, and illumination intensity, respectively. When bimolecular recombination is dominant, s is approximately equal to 1 and reaches 2 in the case of dominant trap-assisted recombination. The s values of the device based on pure ZnO, **2EBr**, and **4PBr** were 1.78, 1.71, and 1.29, respectively. Therefore, the lowest trap-assisted recombination behavior of the device based on **4PBr** can justify its highest J_{sc} and FF values. Overall, most device parameters related to the charge extraction and recombination characteristics of the devices are continuously improved by introducing the interlayer. In addition, the change in the s values of the devices agrees well with the PCE trend of PSCs.

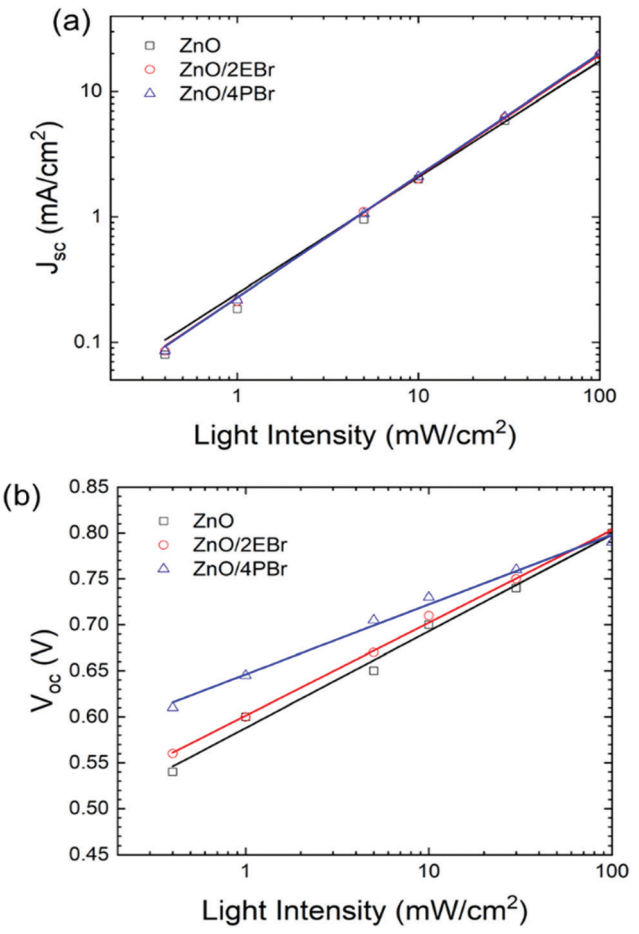

Fig. 5 (a) J_{sc}–light intensity and (b) V_{oc}–light intensity plots of the PSCs.

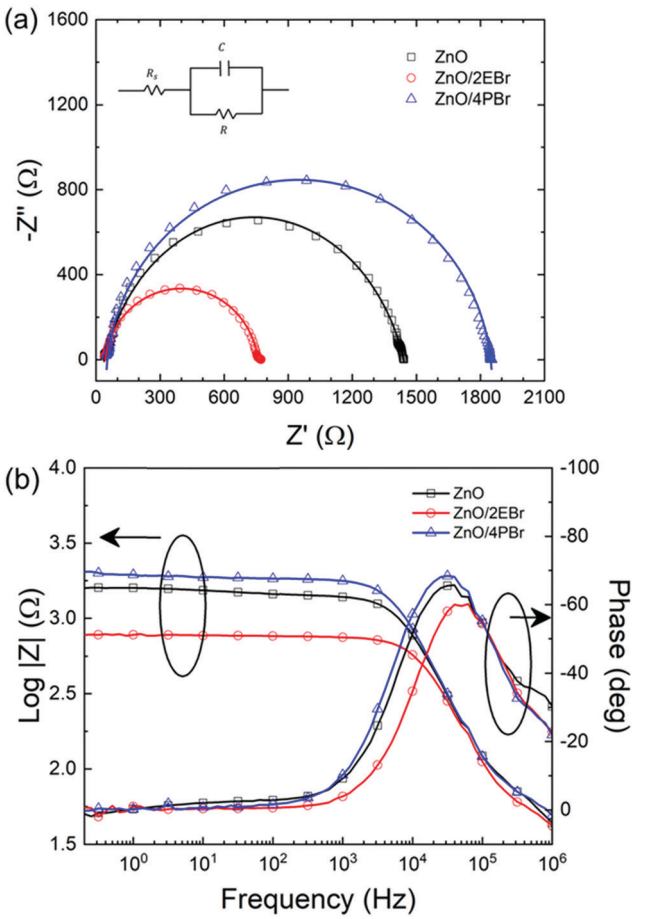

Fig. 6 (a) EIS spectra at 0.8 V under dark conditions, inset shows the equivalent circuit for analysis of EIS spectra (R_s: ohmic resistance including the electrodes and bulk resistance, R: resistance associated with the interface charge transport, C: capacitance) and (b) Bode plot.

To further observe the carrier recombination and transport mechanism, we examined the electrical impedance spectra (EIS) of the PSCs under dark conditions. EIS measurements were performed at 0 V with a frequency range of 1–1.0 MHz.

Fig. 6a shows the Nyquist plots of the devices at 0.8 V. The EIS spectra were linearly fitted to estimate the recombination resistance (R_{rec}). A single semi-circle without a transmission line was observed in the Nyquist plots of each devices. Its diameter is assigned to the charge transfer resistance.[53,54] The size of the EIS semi-circle reflects the extent of R_{rec}; thus, depending on the extent of the charge recombination PSCs. The magnitude of the R_{rec} of the devices was 1.51, 0.836, and 1.97 kΩ for pristine ZnO, with **2EBr**, and with **4PBr**, respectively. Notably, the device based on ZnO with **4PBr** exhibited the highest R_{rec}, indicating the lowest reduced interfacial recombination. The trend of R_{rec} followed those of the FF and R_{sh} of PSCs. As shown in Fig. 6b, the peak frequency of the devices followed the trend of the FF and R_{sh}. This indicates that the interlayer also modifies the electron lifetime. Moreover, the electron lifetime (τ) can be estimated using the equation $\tau = 1/2\pi f_{mid}$, where f_{mid} is the midfrequency peak of the Bode plot in the impedance spectrum.[53] The estimated τ of the devices based on pristine ZnO, ZnO/**2EBr**, and ZnO/**4PBr** was 25, 13, and 32 μs, respectively. This result supports the EIS analysis results.

Conclusions

Small-molecule electrolytes, **2EBr** and **4PBr**, have been successfully synthesized. The PSCs with **2EBr** exhibited an enhanced PCE, reaching up to 9.56%. The PCE was further enhanced by using **4PBr** as the interlayer due to the increased ion size and number of ionic functionalities. The enhanced PCE can be mainly attributed to the improvement of J_{sc}. In addition, the trend of the FF followed that of PCEs. The charge-generation, charge-transport, and charge-recombination characteristics also supported the PCE enhancement. As a result, we demonstrated the possibility of maximizing the performances without complicated synthesis procedures.

Conflicts of interest

There are no conflicts to declare.

Acknowledgements

This research work was supported by the New & Renewable Energy Core Technology Program of the Korea Institute of Energy Technology Evaluation and Planning (KETEP) granted financial resource from the Ministry of Trade, Industry & Energy, Republic of Korea (20193091010110) and was supported by the Basic Science Research Program through the National Research Foundation of Korea (NRF) funded by the Ministry of Education (2019R1A2C1002585).

Notes and references

1 G. Yu, J. Gao, J. C. Hummelen, F. Wudl and A. J. Heeger, *Science*, 1995, **270**, 1789.
2 S. Gunes, H. Neugebauer and N. S. Sariciftci, *Chem. Rev.*, 2007, **107**, 1324.
3 L. Lu, T. Zheng, Q. Wu, A. M. Schneider, D. Zhao and L. Yu, *Chem. Rev.*, 2015, **115**, 12666.
4 Y.-W. Su, S.-C. Lan and K.-H. Wei, *Mater. Today*, 2012, **15**, 554.
5 J. Yuan, Y. Zhang, L. Zhou, H.-L. Yip, T.-K. Lau, X. Lu, C. Zhu, H. Peng, P. A. Johnson, M. Leclerc, Y. Cao, J. Ulanski, Y. Li and Y. Zou, *Joule*, 2019, **3**, 1140–1151.
6 X. Li, X. Liu, W. Zhang, H.-Q. Wang and J. Fang, *Chem. Mater.*, 2017, **29**, 4176–4180.
7 Z. Wu, C. Sun, S. Dong, X.-F. Jiang, S. Wu, H. Wu, H.-L. Yip, F. Huang and Y. Cao, *J. Am. Chem. Soc.*, 2016, **138**, 2004–2013.
8 M. Lv, S. Li, J. J. Jasieniak, J. Hou, J. Zhu, Z. Tans, S. E. Watkins, Y. Li and X. Chen, *Adv. Mater.*, 2013, **25**, 6889–6894.
9 C. J. Brabec, A. Cravino, D. Meissner, N. S. Sariciftci, T. Fromherz, M. T. Rispens, L. Sanchez and J. C. Hummelen, *Adv. Funct. Mater.*, 2001, **11**, 374–380.
10 Y. Li, *Acc. Chem. Res.*, 2012, **45**, 723–733.
11 W. Zhang, Y. Wu, Q. Bao, F. Gao and J. Fang, *Adv. Energy Mater.*, 2014, **4**, 1400359.
12 G. Yu, J. Gao, J. C. Hummelen, F. Wudl and A. J. Heeger, *Science*, 1995, **270**, 1789–1791.
13 M. H. Hoang, G. E. Park, D. L. Phan, T. T. Ngo, T. V. Nguyen, C. G. Park, M. J. Cho and D. H. Choi, *Macromol. Res.*, 2018, **26**, 844–850.
14 Y. J. Lee, S. J. Jeon, J. Y. Choi and D. K. Moon, *J. Ind. Eng. Chem.*, 2019, **75**, 138–147.
15 B. Zhu, X. Chen, S. I. Huang and X. Peng, *Dyes Pigm.*, 2019, **164**, 148–155.
16 S. S. Badge, H. Park, V. H. Tran and S. H. Lee, *Dyes Pigm.*, 2019, **163**, 30–39.
17 S.-H. Oh, S.-I. Na, J. Jo, B. Lim, D. Vak and D.-Y. Kim, *Adv. Funct. Mater.*, 2010, **20**, 1977.
18 S. Nho, G. Baek, S. Park, B. R. Lee, M. J. Cha, D. C. Lim, J. H. Seo, S.-H. Oh, M. H. Song and S. Cho, *Energy Environ. Sci.*, 2016, **9**, 240.
19 Y. Sun, J. H. Seo, C. J. Takacs, J. Seifter and A. J. Heeger, *Adv. Mater.*, 2011, **23**, 1679.
20 C. E. Small, S. Chen, J. Subbiah, C. M. Amb, S.-W. Tsang, T.-H. Lai, J. R. Reynolds and F. So, *Nat. Photonics*, 2012, **6**, 115.
21 M. Y. Jo, Y. E. Ha and J. H. Kim, *Sol. Energy Mater. Sol. Cells*, 2012, **107**, 1.
22 M. Y. Jo, Y. E. Ha and J. H. Kim, *Org. Electron.*, 2013, **14**, 995.
23 G. E. Lim, Y. E. Ha, M. Y. Jo, J. Park, Y.-C. Kang and J. H. Kim, *ACS Appl. Mater. Interfaces*, 2013, **5**, 6508.
24 Y. Li, X. Liu, X. Li, W. Zhang, F. Xing and J. Fang, *ACS Appl. Mater. Interfaces*, 2017, **9**, 8426.
25 Z. Li, Q. Chen, Y. Liu, L. Ding, K. Zhang, K. Zhu, L. Yuan, B. Dong, Y. Zhou and B. Song, *Macromol. Rapid Commun.*, 2018, **39**, 1700828.
26 Y. H. Kim, N. Sylvianti, M. A. Marsya, J. Park, Y.-C. Kang, D. K. Moon and J. H. Kim, *ACS Appl. Mater. Interfaces*, 2016, **8**, 32992.

27 Y. H. Kim, N. Sylvianti, M. A. Marsya, D. K. Moon and J. H. Kim, *Org. Electron.*, 2016, **39**, 163.
28 X. Guo, Y. Zhang, X. Liu, S. Braun, Z. Wang, B. Li, Y. Li, C. Duan, M. Fahlman, J. Tang, J. Fang and Q. Bao, *Org. Electron.*, 2018, **59**, 15.
29 J. P. Han, E. J. Lee, Y. W. Han, T. H. Lee and D. K. Moon, *J. Ind. Eng. Chem.*, 2016, **36**, 44.
30 M. Gupta, D. Yan, J. Xu, J. Yao and C. Zhan, *ACS Appl. Mater. Interfaces*, 2018, **10**, 5569.
31 H.-C. Chen, S.-W. Lin, J.-M. Jiang, Y.-W. Su and K.-H. Wei, *ACS Appl. Mater. Interfaces*, 2015, **7**, 6273.
32 S.-H. Liao, H.-J. Jhuo, Y.-S. Cheng and S.-A. Chen, *Adv. Mater.*, 2013, **25**, 4766.
33 H. Yang, T. Wu, T. Hu, X. Hu, L. Chen and Y. Chen, *J. Mater. Chem. C*, 2016, **4**, 8738.
34 X. Li, X. Liu, W. Zhang, H.-Q. Wang and J. Fang, *Chem. Mater.*, 2017, **29**, 4176.
35 Y. H. Kim, D. G. Kim and J. H. Kim, *Appl. Chem. Chem. Eng.*, 2016, **27**, 512.
36 T. T. Do, H. S. Hong, Y. E. Ha, J. Park, Y.-C. Kang and J. H. Kim, *ACS Appl. Mater. Interfaces*, 2015, **7**, 3335.
37 T. T. Do, H. S. Hong, Y. E. Ha, C.-Y. Park and J. H. Kim, *Macromol. Res.*, 2015, **23**, 177.
38 R. Peng, Z. Liu, Q. Guan, L. Hong, W. Song, Q. Wei, P. Gao, J. Huang, X. Fan, M. Wang and Z. Ge, *J. Mater. Chem. A*, 2018, **6**, 6327–6334.
39 X. Ouyang, R. Peng, L. Ai, X. Zhang and Z. Ge, *Nat. Photonics*, 2015, **9**, 520–524.
40 Z. Liu, X. Ouyang, R. Peng, Y. Bai, D. Mi, W. Jiang, A. Facchetti and Z. Ge, *J. Mater. Chem. A*, 2016, **4**, 2530–2536.
41 X. Li, W. Zhang, X. Wang, Y. Wu, F. Cao and J. Fang, *J. Mater. Chem. A*, 2015, **4**, 504–508.
42 Y. H. Kim, D. G. Kim, R. D. Maduwu, H. C. Jin, D. K. Moon and J. H. Kim, *Sol. RRL*, 2018, **2**, 1800086.
43 D. G. Kim, Y. H. Kim, R. D. Maduwu, H. C. Jin, D. K. Moon and J. H. Kim, *J. Ind. Eng. Chem.*, 2018, **65**, 175–179.
44 Y. H. Kim, N. Sylvianti, M. A. Marsya, J. Park, Y.-C. Kang, D. K. Moon and J. H. Kim, *ACS Appl. Mater. Interfaces*, 2016, **8**, 32992–32997.
45 M. Jeong, H. C. Jin, D. K. Moon and J. H. Kim, *Adv. Mater. Interfaces*, 2019, **6**, 1900797.
46 M. Jeong, H. C. Jin, D. K. Moon and J. H. Kim, *Dyes Pigm.*, 2020, **173**, 107927.
47 B. H. Lee, I. H. Jung, H. Y. Woo, H. K. Shim, G. Kim and K. K. Lee, *Adv. Funct. Mater.*, 2014, **24**, 1100–1108.
48 M. Y. Jo, Y. E. Ha, Y. S. Won, S. I. Yoo and J. H. Kim, *Org. Electron.*, 2015, **25**, 85–91.
49 I. D. Parker, *J. Appl. Phys.*, 1994, **75**, 1656.
50 F. Yang, Y. Xu, M. Gu, S. Zhou, Y. Wang, K. Lu, Z. Liu, X. Ling, Z. Zhu, J. Chen, Z. Wu, Y. Zhang, Y. Xue, F. Li, J. Yuan and W. Ma, *J. Mater. Chem. A*, 2018, **6**, 17688–17697.
51 R. Azmi, S.-H. Oh and S.-Y. Jang, *ACS Energy Lett.*, 2016, **1**, 100–106.
52 L. J. A. Koster, V. D. Mihailetchi, R. Ramaker and P. W. M. Blom, *Appl. Phys. Lett.*, 2005, **86**, 123509.
53 H. Kim, H. Jeong, T. K. An, C. E. Park and K. Yong, *ACS Appl. Mater. Interfaces*, 2013, **5**, 268–275.
54 H. Wang, G. Liu, X. Li, P. Xiang, Z. Ku, Y. Rong, M. Xu, L. Liu, M. Hu, Y. Yang and H. Han, *Energy Environ. Sci.*, 2011, **4**, 2025–2029.